


 Cite this: *RSC Adv.*, 2022, 12, 11190

# Revealing the different performance of $\text{Li}_4\text{SiO}_4$ and $\text{Ca}_2\text{SiO}_4$ for $\text{CO}_2$ adsorption by density functional theory†

 Wenjing Yu,<sup>a</sup> Qian Xu,<sup>\*a</sup> Shenggang Li,<sup>b</sup> Xiaolu Xiong,<sup>a</sup> Hongwei Cheng,<sup>a</sup> Xingli Zou<sup>a</sup> and Xiongqiang Lu<sup>a</sup>

To reveal the difference between  $\text{Li}_4\text{SiO}_4$  and  $\text{Ca}_2\text{SiO}_4$  in  $\text{CO}_2$  adsorption performance, the  $\text{CO}_2$  adsorption on  $\text{Li}_4\text{SiO}_4$  (010) and  $\text{Ca}_2\text{SiO}_4$  (100) surfaces was investigated using density functional theory (DFT) calculations. The results indicate that the bent configuration of the adsorbed  $\text{CO}_2$  molecule parallel to the surface is the most thermodynamically favorable for both  $\text{Li}_4\text{SiO}_4$  and  $\text{Ca}_2\text{SiO}_4$  surfaces. The  $\text{Li}_4\text{SiO}_4$  (010) surface has greater  $\text{CO}_2$  adsorption energy ( $E_{\text{ads}} = -2.97$  eV) than the  $\text{Ca}_2\text{SiO}_4$  (100) surface ( $E_{\text{ads}} = -0.31$  eV). A stronger covalent bond between the C atom of adsorbed  $\text{CO}_2$  and an  $\text{O}_5$  atom on the  $\text{Li}_4\text{SiO}_4$  (010) surface is formed, accompanied by more charge transfer from the surface to  $\text{CO}_2$ . Moreover, the Mulliken charge of  $\text{O}_5$  atoms on the  $\text{Li}_4\text{SiO}_4$  (010) surface is more negative, and its p-band center is closer to the  $E_f$ , indicating  $\text{O}_5$  atoms on  $\text{Li}_4\text{SiO}_4$  (010) are more active and prone to suffering electrophilic attack compared with the  $\text{Ca}_2\text{SiO}_4$  (100) surface.

Received 16th February 2022

Accepted 4th April 2022

DOI: 10.1039/d2ra01021f

[rsc.li/rsc-advances](https://rsc.li/rsc-advances)

## 1. Introduction

$\text{CO}_2$  capture, storage and utilization (CCSU) is considered as one of the most promising technologies for reducing anthropogenic  $\text{CO}_2$  emission, which can lead to global warming. Solid inorganic sorbents have been proven to efficiently remove  $\text{CO}_2$  at high temperatures, and are more economical and effective than low-temperature amine-based materials in  $\text{CO}_2$  capture from high temperature exhaust gas.<sup>1</sup> Lithium orthosilicate ( $\text{Li}_4\text{SiO}_4$ ) is one of the best  $\text{CO}_2$  capture sorbents due to its significant advantages, such as large adsorption capacity, low regeneration temperature, and good adsorption and desorption cycle stability.<sup>2–4</sup> There have been a lot of experimental studies on  $\text{Li}_4\text{SiO}_4$  as an adsorbent to capture  $\text{CO}_2$ , including the synthesis method,<sup>5,6</sup> kinetic behavior<sup>7–9</sup> and modification of  $\text{Li}_4\text{SiO}_4$ .<sup>10–12</sup> However, lithium is relatively expensive and not very abundant in the earth's crust. In particular, lithium batteries have been widely used as a source of power or energy for a lot of things from portable electronics to electric vehicles. As a result, the demand for lithium is increased which leads directly to an increase of its price. Accordingly, it is very difficult to apply lithium-based ceramics on a huge scale to capture  $\text{CO}_2$  economically and sustainably. Meanwhile there are abundant resources basic silicates all over the world, especially calcium silicates ( $\text{Ca}_2\text{SiO}_4$ ) are often found in the industrial by-products

named as slags generated during iron and steel production. Furthermore,  $\text{Ca}_2\text{SiO}_4$ , similar to  $\text{Li}_4\text{SiO}_4$ , is thermodynamically favorable for  $\text{CO}_2$  capture from room temperature to 572 °C at ambient pressure, and Gibbs free energy changes for the carbonation of  $\text{Ca}_2\text{SiO}_4$  and  $\text{Li}_4\text{SiO}_4$  were calculated by HSC Chemistry 6.0 and shown in Fig. 1. However, the slow diffusion and reaction of carbonation between  $\text{CO}_2$  and calcium silicates is a common issue even at high temperatures in the case of no participation of water.<sup>13</sup> It was found that the amount of  $\text{CO}_2$  captured with  $\text{Ca}_2\text{SiO}_4$  is little at the temperature range from room temperature to 572 °C in our previous study. Zhao *et al.*<sup>14,15</sup> applied  $\text{Ca}_2\text{SiO}_4$  as the inert material to enhance the sintering resistance and cyclic stability of CaO during multiple sorption/desorption of  $\text{CO}_2$ . It could be deduced that  $\text{Ca}_2\text{SiO}_4$  is much inerte for carbonation compared with  $\text{Li}_4\text{SiO}_4$  at the high temperatures.

The investigation on the effect of the electronic structure of the silicates on their carbonation reactivity should be very important for understanding deeply the different carbonation behaviors for  $\text{Li}_4\text{SiO}_4$  and  $\text{Ca}_2\text{SiO}_4$ , and developing new approaches to improve the carbonation activity of silicates.

There are some investigations about  $\text{CO}_2$  adsorption on the surface of the oxides and silicates with the first-principles calculations. Kim *et al.*<sup>16</sup> made an assessment of  $\text{Li}_2\text{O}$  and  $\text{Na}_2\text{O}$  surfaces for  $\text{CO}_2$  adsorption based on DFT calculations. They found that the introduction of dopant atoms larger than host metal atoms of the surfaces can negatively increase  $\text{CO}_2$  adsorption energies. Kumar *et al.*<sup>17</sup> studied the  $\text{CO}_2$  adsorption on different terminations of  $\text{Cr}_2\text{O}_3$  surfaces with DFT calculations and found that carboxylate species are formed on O layer

<sup>a</sup>Shanghai University, China

<sup>b</sup>Shanghai Advanced Research Institute, China

 † Electronic supplementary information (ESI) available. See <https://doi.org/10.1039/d2ra01021f>

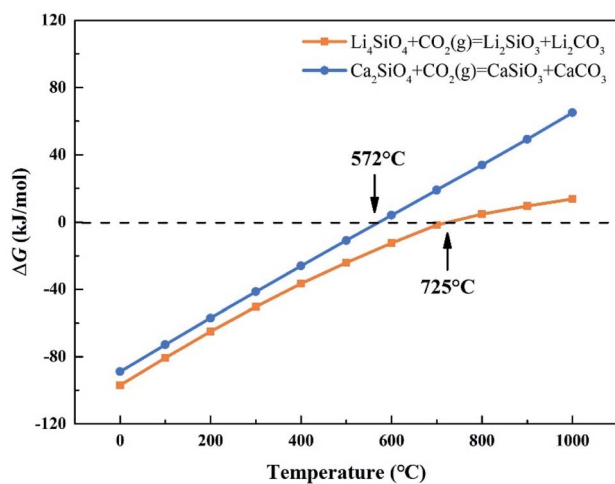



Fig. 1 Relationship between  $\Delta G$  and temperature of carbonation reaction between  $\text{CO}_2$  and  $\text{Li}_4\text{SiO}_4$  and  $\text{Ca}_2\text{SiO}_4$ .

terminated-(0001), and carbonate species are formed on O layer terminated-(10 $\bar{1}$ 2) and Cr layer terminated-(01 $\bar{1}$ 2), indicating that the formation of physisorbed and chemisorbed species depends on different surface terminations. Kang *et al.*<sup>18</sup> thermodynamically evaluated the  $\text{CO}_2$  capture potential of  $\text{Mg}_2\text{MO}_4$  ( $\text{M} = \text{Si}, \text{V}, \text{and Ge}$ ). Their results indicated that the critical temperature at which  $\text{CO}_2$  can be absorbed, increased with decreasing Pauling electronegativity of the M site.

There are several investigations for  $\text{Li}_4\text{SiO}_4$  on its structural, electronic, lattice dynamical and thermodynamic properties. Duan<sup>19</sup> and Tang *et al.*<sup>20</sup> found the covalency properties of  $\text{Li}_4\text{SiO}_4$  mainly resulting from the overlap of O 2p and Si 3p orbitals. Kong *et al.*<sup>21</sup> studied the adsorption mechanism of  $\text{H}_2\text{O}$  on the  $\text{Li}_4\text{SiO}_4$  (010) surface. It was suggested an interaction between adsorbed  $\text{H}_2\text{O}$  and  $\text{Li}_4\text{SiO}_4$  (010) surface, including an electrophilic interaction of hydrogen atom in water with oxygen

atoms on the surface and a nucleophilic interaction of oxygen atoms in water with Li atoms on the surface.

$\text{Ca}_2\text{SiO}_4$ , as the industrial cement clinkers, has been investigated by DFT calculations extensively, and many studies focused on the hydration of  $\text{Ca}_2\text{SiO}_4$  phases. Qi *et al.*<sup>22</sup> investigated  $\text{H}_2\text{O}$  adsorption on low-index surfaces of  $\text{Ca}_2\text{SiO}_4$ , indicating that electron are mainly transferred from surface atoms to  $\text{H}_2\text{O}$  molecule. Wang *et al.*<sup>23</sup> evaluated  $\text{H}_2\text{O}$  adsorption on  $\beta$ - $\text{Ca}_2\text{SiO}_4$  surfaces and found a dual interaction between  $\text{H}_2\text{O}$  and  $\beta$ - $\text{Ca}_2\text{SiO}_4$  (100) surface. Wang *et al.*<sup>24</sup> also studied the relationship between reactivity and electronic structure of  $\alpha'_L$ -,  $\beta$ - and  $\gamma$ - $\text{Ca}_2\text{SiO}_4$  for hydration process. They found that the higher hydration reactivity of  $\alpha'_L$ - and  $\beta$ - $\text{Ca}_2\text{SiO}_4$  compared with  $\gamma$ - $\text{Ca}_2\text{SiO}_4$  are attributed to the higher charge density and larger local state density of the active oxygen atoms in  $\alpha'_L$ - and  $\beta$ - $\text{Ca}_2\text{SiO}_4$ . However, there are few investigations about explanation of the different behaviors of carbonation of  $\text{Ca}_2\text{SiO}_4$  and  $\text{Li}_4\text{SiO}_4$  on the base of their structural and electronic properties.

Herein, we have systematically investigated the structural and electronic properties of  $\text{Li}_4\text{SiO}_4$  and  $\text{Ca}_2\text{SiO}_4$ , and the adsorption of  $\text{CO}_2$  on the most stable surfaces of  $\text{Li}_4\text{SiO}_4$  and  $\text{Ca}_2\text{SiO}_4$  on the base of density functional theory calculations. We tried to reveal the relationship between the electronic structures of  $\text{Li}_4\text{SiO}_4$  and  $\text{Ca}_2\text{SiO}_4$  and their reactivity for  $\text{CO}_2$  adsorption on the molecular scale. The results of this investigation could converge to a proposed mechanism of  $\text{CO}_2$  capture with the orthosilicates, on which the more reactive silicates for  $\text{CO}_2$  capture can be screened out as the candidates for  $\text{CO}_2$  capture.

## 2. Computational details

The calculations were performed based on density functional theory (DFT), using Cambridge Series Total Energy Package (CASTEP) code.<sup>25</sup> The exchange-correlation potential was approximated within the generalized gradient approximation

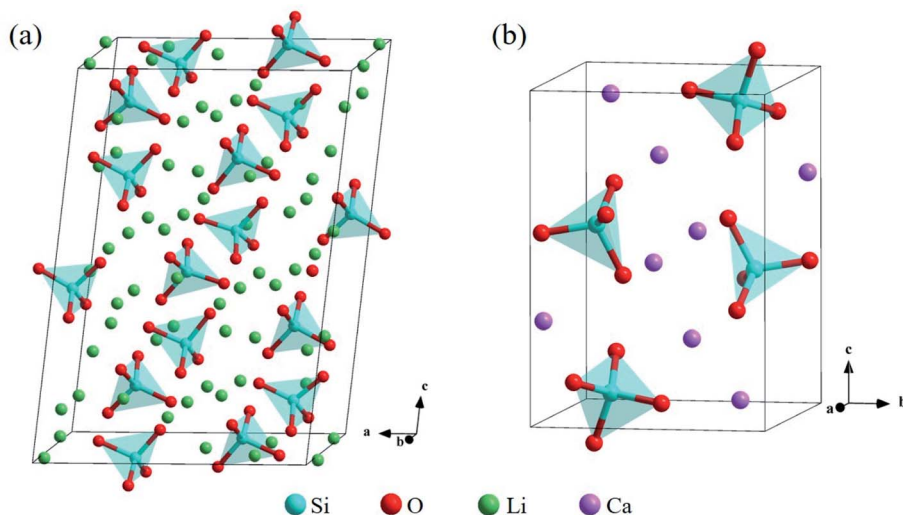


Fig. 2 Crystal structures of (a)  $\text{Li}_4\text{SiO}_4$  and (b)  $\text{Ca}_2\text{SiO}_4$ . The Si, O, Li and Ca atoms are shown by blue, red, green and purple spheres, respectively.



**Table 1** Comparison of calculated lattice constants of  $\text{Li}_4\text{SiO}_4$  and  $\text{Ca}_2\text{SiO}_4$  with experimental lattice constants

	$\text{Li}_4\text{SiO}_4$			$\text{Ca}_2\text{SiO}_4$		
	Cal	Expt <sup>19</sup>	$\Delta$ (%)	Cal	Expt <sup>40</sup>	$\Delta$ (%)
$a$ (Å)	11.511	11.532	0.18	5.571	5.502	1.25
$b$ (Å)	6.080	6.075	0.08	6.800	6.745	0.82
$c$ (Å)	16.708	16.678	0.18	9.354	9.297	0.61
$\beta$ (°)	99.15	99.04	0.11	94.295	94.590	0.31

(GGA)<sup>26</sup> using the Perdew–Burke–Ernzerhof (PBE) functional.<sup>27</sup> Dispersion-corrected calculations<sup>28</sup> were performed with Grimme's DFT-D3 methodology.<sup>29</sup> To model  $\text{Li}_4\text{SiO}_4$  and  $\text{Ca}_2\text{SiO}_4$ , the unit cell ( $1 \times 1 \times 1$ ) was applied for the calculation.

In order to optimize the crystal structures, the plane wave truncation energy and k-points were tested. A cutoff-energy of 650 eV was used for plane wave expansions. The k-points meshes within Monkhorst-Pack<sup>30</sup> framework were set as  $3 \times 6 \times 2$  and  $4 \times 3 \times 2$  for  $\text{Li}_4\text{SiO}_4$  and  $\text{Ca}_2\text{SiO}_4$  respectively. The Broyden–Fletcher–Goldfarb–Shanno (BFGS)<sup>31</sup> minimization algorithm was used to optimize the primitive unit cell. The surfaces of  $\text{Li}_4\text{SiO}_4$  and  $\text{Ca}_2\text{SiO}_4$  were cleaved from the optimized bulk structure. All surfaces were kept stoichiometric and neutral to avoid the polarizing electric field. The thicknesses of vacuum layer were set as 15 Å to avoid the interaction between

slabs. The convergence criteria were fixed, specifically: the energy change within  $1 \times 10^{-5}$  eV per atom, the force on the atoms within  $0.03 \text{ eV } \text{Å}^{-1}$ , the stress on the atoms within 0.05 GPa, and the displacement of atoms within  $1 \times 10^{-3}$  Å. All the initial crystal structures and data were obtained from the Inorganic Crystal Structure Database (ICSD).<sup>32</sup>

## 3. Results and discussion

### 3.1. Structural and electronic properties of bulks

The bulk structure of  $\text{Li}_4\text{SiO}_4$  with the monoclinic phase, which space group is  $P21/m$  (no. 11),<sup>33–35</sup> was optimized. The unit cell of  $\text{Li}_4\text{SiO}_4$  contains 126 atoms, including 14  $[\text{SiO}_4]^{4-}$  tetrahedra and 56 Li atoms, as shown in Fig. 2a, which are centrally symmetrical. Meanwhile, the bulk structure of  $\text{Ca}_2\text{SiO}_4$  with the monoclinic phase, which space group is  $P21/n$  (no. 14),<sup>36–38</sup> was optimized as well. The unit cell of  $\text{Ca}_2\text{SiO}_4$  consists of 28 atoms, including 4  $[\text{SiO}_4]^{4-}$  tetrahedra and 8 Ca atoms, as shown in Fig. 2b. The calculated and experimentally measured lattice parameters of  $\text{Li}_4\text{SiO}_4$  and  $\text{Ca}_2\text{SiO}_4$  are presented in Table 1, and they are in good agreement, implying the simulation settings are reliable and give reasonable results.

Fig. 3 shows the total density of states (TDOS) and partial density of states (PDOS) for  $\text{Li}_4\text{SiO}_4$  and  $\text{Ca}_2\text{SiO}_4$ . Electrons occupying the orbitals below and near the Fermi level ( $E_f$ ) is of great significance to the activity of the crystal materials for chemical reactions,<sup>39</sup> so we focused on the electrons on the

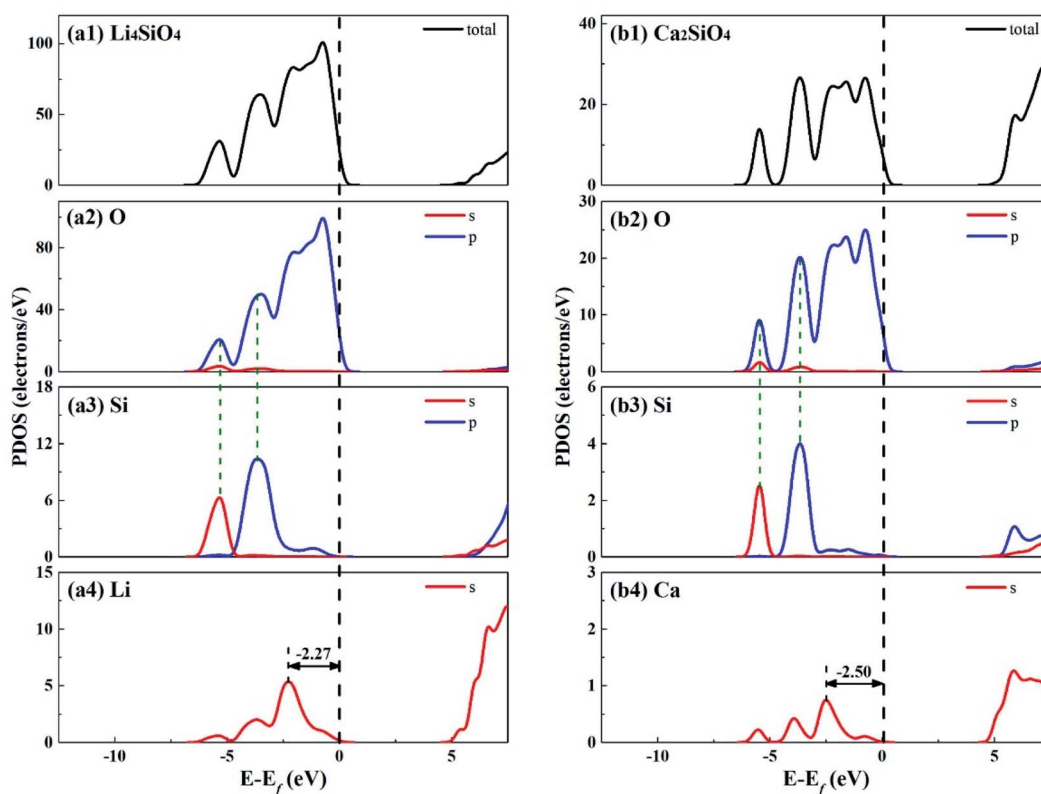


**Fig. 3** DOS analysis for (a)  $\text{Li}_4\text{SiO}_4$  and (b)  $\text{Ca}_2\text{SiO}_4$ . The black dashed line shows the Fermi level.



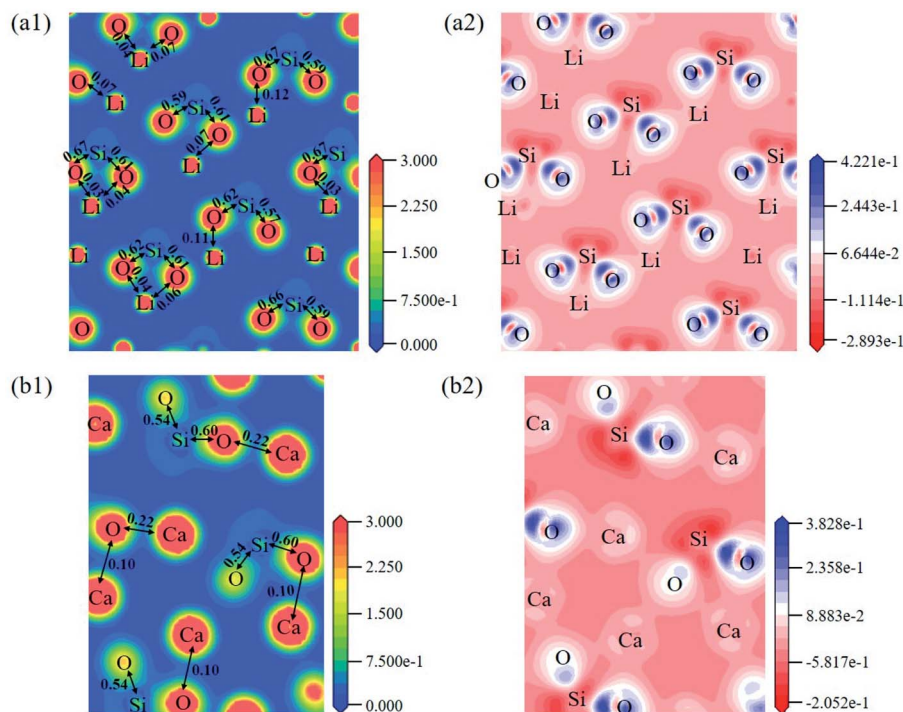


Fig. 4 Contour maps of electron density distributions and differential charge density of (a)  $\text{Li}_4\text{SiO}_4$  in the plane (010) and (b)  $\text{Ca}_2\text{SiO}_4$  in the plane (100).

Table 2 The surface energies ( $E_{\text{surf}}$  in  $\text{J m}^{-2}$ ) of low Miller index surfaces of  $\text{Li}_4\text{SiO}_4$  and  $\text{Ca}_2\text{SiO}_4$

Surface	(100)	(010)	(001)	(110)	(101)	(011)	(111)
$\text{Li}_4\text{SiO}_4$	1.28	0.78	1.34	0.80	1.28	0.87	0.84
$\text{Ca}_2\text{SiO}_4$	0.63	1.19	0.80	0.86	0.66	0.75	0.82

orbitals below and near the  $E_f$ . For  $\text{Li}_4\text{SiO}_4$  and  $\text{Ca}_2\text{SiO}_4$ , their TDOS near the  $E_f$  is mainly contributed by the p orbitals of O atoms, suggesting that O atoms are more active and more likely serve as the electron donors. Their PDOS in the region between  $-6.55 \sim -2.92$  eV and  $-6.25 \sim -3.02$  eV are overlapped with the

Si s and p bands, implying orbital hybridization and Si-O binding in the bulks of  $\text{Li}_4\text{SiO}_4$  and  $\text{Ca}_2\text{SiO}_4$ . However, the states in the region between  $-3$  and  $0$  eV, near to  $E_f$  is about 73% of the total PDOS for O p orbitals for  $\text{Li}_4\text{SiO}_4$ , while that for  $\text{Ca}_2\text{SiO}_4$  is about 70%. It can be deduced that there are more electronic states for O p orbitals below and near to  $E_f$  in  $\text{Li}_4\text{SiO}_4$  than those in  $\text{Ca}_2\text{SiO}_4$ , Then the electron transfer from O atoms occurs more easier in  $\text{Li}_4\text{SiO}_4$  than in  $\text{Ca}_2\text{SiO}_4$ .

Furthermore, the first high peak position<sup>41</sup> in the PDOS for Li s orbital of  $\text{Li}_4\text{SiO}_4$ , is closer to the  $E_f$  compared with that for Ca s orbital of  $\text{Ca}_2\text{SiO}_4$ , implying that the outer electron of Li

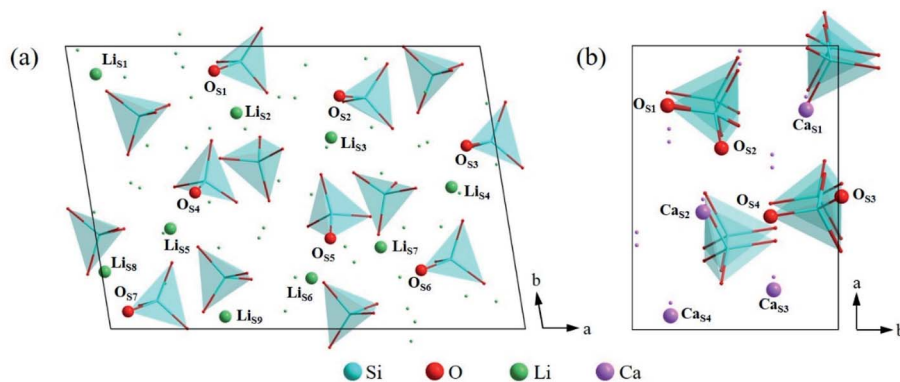


Fig. 5 Atomic arrangement of (a)  $\text{Li}_4\text{SiO}_4$  (010) surface and (b)  $\text{Ca}_2\text{SiO}_4$  (100) surface from the top view. The lines and dots represent the underlying atoms and tetrahedra respectively.



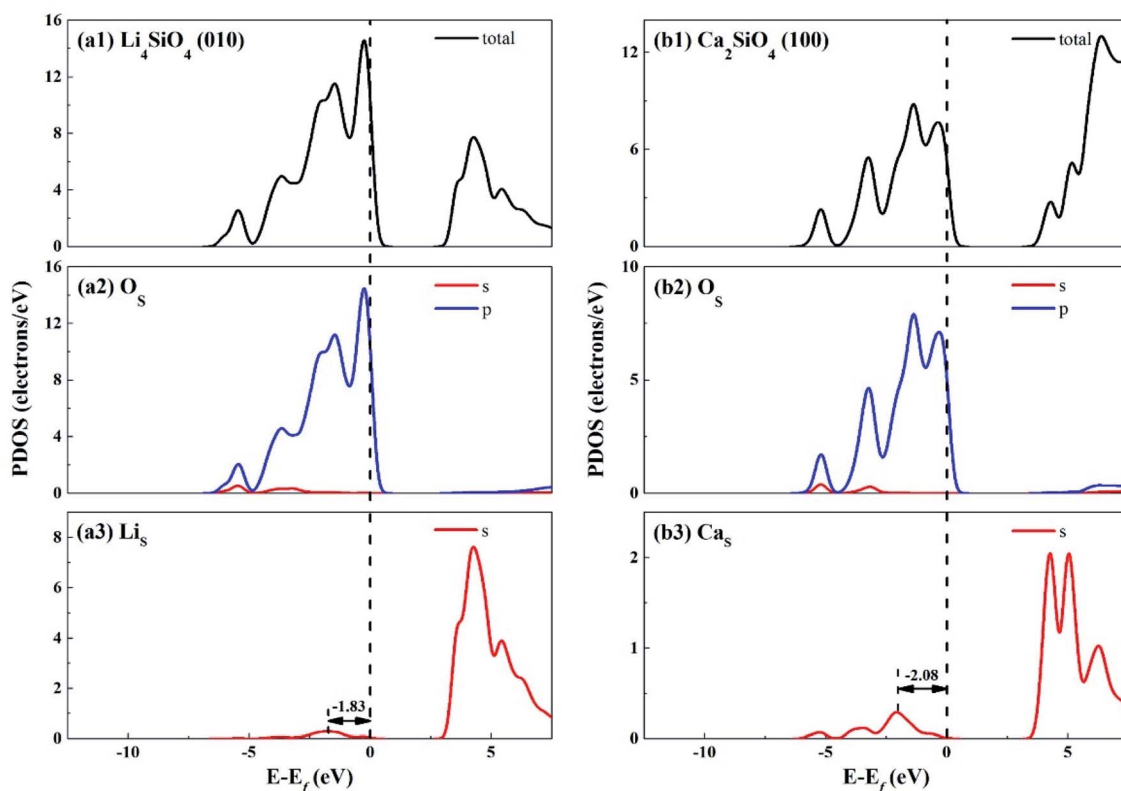


Fig. 6 DOS analysis of the topmost surface layers of (a)  $\text{Li}_4\text{SiO}_4$  (010) surface and (b)  $\text{Ca}_2\text{SiO}_4$  (100) surface without  $\text{CO}_2$  adsorption. The black dashed line shows the Fermi level.

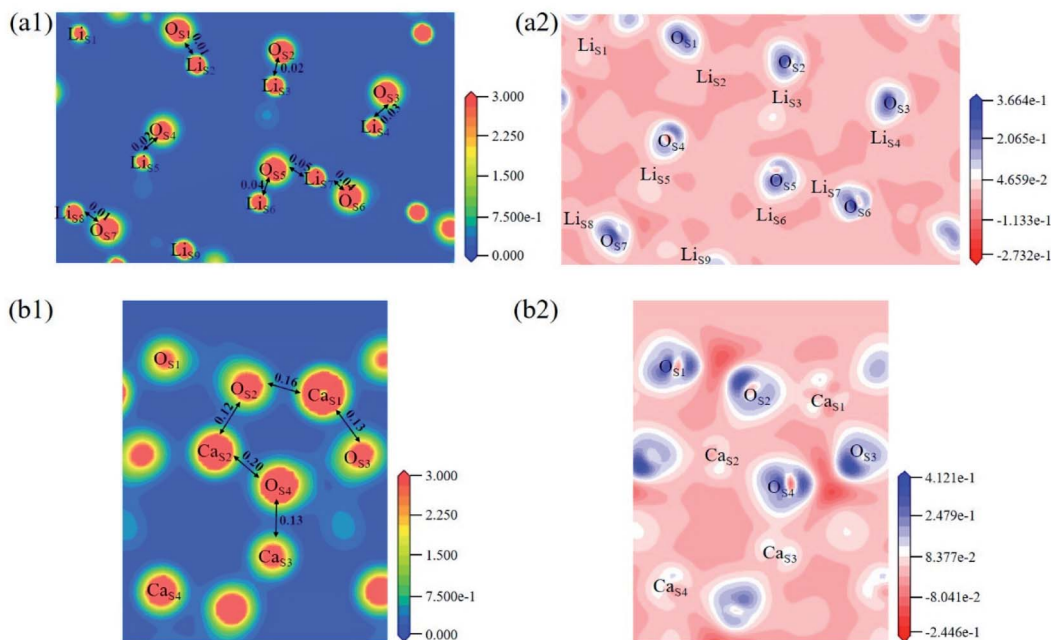


Fig. 7 Contour maps of electron density distributions and differential charge density in the cross sections perpendicular to the (001) plane in (a)  $\text{Li}_4\text{SiO}_4$  (010) surface and (b)  $\text{Ca}_2\text{SiO}_4$  (100) surface.



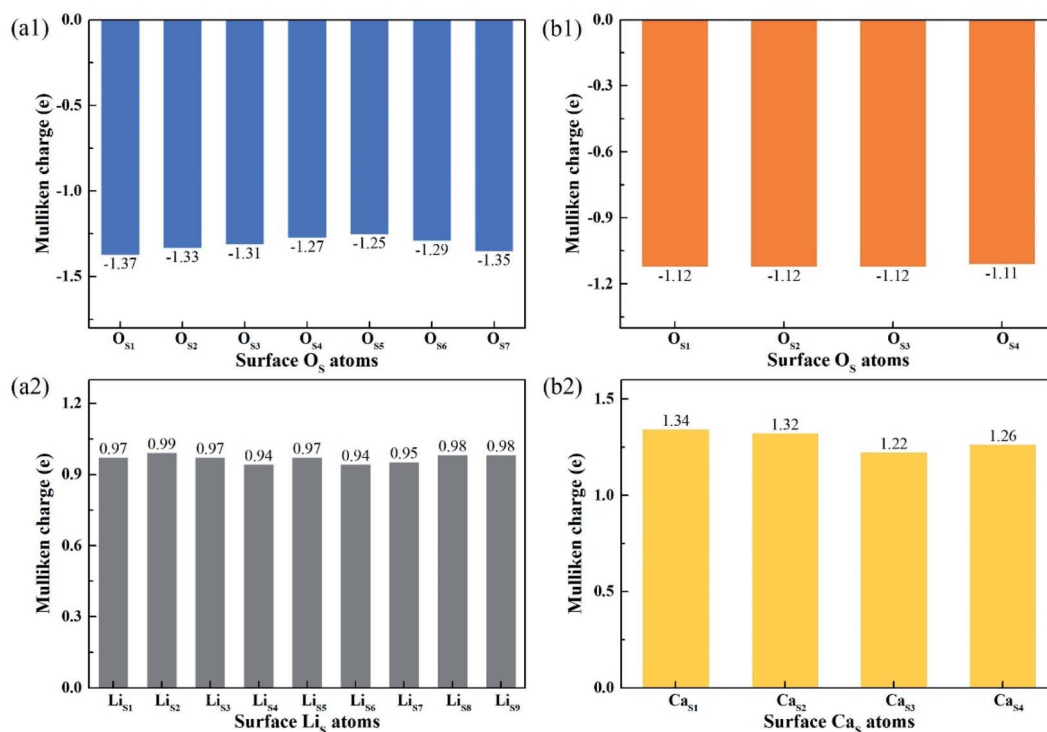


Fig. 8 Mulliken charge analysis of atoms on the topmost surface layers of (a)  $\text{Li}_4\text{SiO}_4$  (010) surface and (b)  $\text{Ca}_2\text{SiO}_4$  (100) surface.

atoms in  $\text{Li}_4\text{SiO}_4$  can be transferred away easier than Ca atoms in  $\text{Ca}_2\text{SiO}_4$ .

The electron density distribution can show the bonding between atoms and differential charge density can show the accumulation and depletion of electrons. In Fig. 4a, electron density between Si and O atoms is higher than surrounding and electrons accumulate in the middle of Si and O atoms, demonstrating that a covalent interaction of Si–O. And according to the charge population marked in the figure, the Si–O covalent interaction is stronger in  $\text{Li}_4\text{SiO}_4$ . Li/Ca–O have a certain covalent interaction and the strength of interaction of Li–O is weaker than Ca–O.

### 3.2. Structural and electronic properties of surfaces

In order to find out the most stable surface, the surface energies of seven low Miller index surfaces were calculated. The surface energy ( $E_{\text{surf}}$ ) can be calculated according to the eqn (1):<sup>42,43</sup>

$$E_{\text{surf}} = (E_{\text{slab}} - nE_{\text{bulk}})/2A \quad (1)$$

where  $E_{\text{slab}}$  and  $E_{\text{bulk}}$  are the total energy of relaxed slab model and unit cell, respectively.  $n$  is the number of formula units contained in the slab.  $A$  is the area of the slab. According to the calculation results listed in Table 2, the (010) surface and (100) surface were the most stable surface of  $\text{Li}_4\text{SiO}_4$  and  $\text{Ca}_2\text{SiO}_4$  respectively, due to their lowest values of surface energy, which is consistent with the previous calculations.<sup>21,22,42</sup> Fig. 5 shows the atomic arrangement of these two surfaces from the top view. The topmost surface layer consists of Li and O atoms for

$\text{Li}_4\text{SiO}_4$ , and Ca and O atoms for  $\text{Ca}_2\text{SiO}_4$ . The atoms of Li, Ca, and O on the topmost surface layer are referred to as  $\text{Li}_s$ ,  $\text{Ca}_s$  and  $\text{O}_s$  hereafter, respectively.

The electronic properties of the surfaces should differ from those of the bulks due to the dangling bonds or surface reconstruction. The electronic properties of  $\text{Li}_4\text{SiO}_4$  (010) surface and  $\text{Ca}_2\text{SiO}_4$  (100) surface were calculated as well. Fig. 6 shows the TDOS and PDOS of the topmost surface layers of  $\text{Li}_4\text{SiO}_4$  (010) surface and  $\text{Ca}_2\text{SiO}_4$  (100) surface. Although the surface TDOS resemble the bulk TDOS shown in Fig. 3 for both  $\text{Li}_4\text{SiO}_4$  and  $\text{Ca}_2\text{SiO}_4$ , the states of  $\text{O}_s$  p orbitals are shifted up in energy, and the states in the region between  $-3$  and  $0$  eV are about 79% of the total PDOS for  $\text{O}_s$  p orbitals for  $\text{Li}_4\text{SiO}_4$  (010) surface, while that for  $\text{Ca}_2\text{SiO}_4$  (100) surface is about 77%. Furthermore, p-band center of  $\text{O}_s$  atoms increased to  $-1.725$  eV from  $-1.936$  eV of O atoms in bulk  $\text{Li}_4\text{SiO}_4$ , and  $-1.939$  eV from  $-2.103$  eV in bulk  $\text{Ca}_2\text{SiO}_4$ . It can be deduced that the reactivity of the surface  $\text{O}_s$  atoms is enhanced compared with the O atoms in the bulks. Considering the states near to  $E_f$  and the p-band center levels, the  $\text{O}_s$  atoms in  $\text{Li}_4\text{SiO}_4$  (010) surface are more prone to suffer the electrophilic attacks with respect to  $\text{Ca}_2\text{SiO}_4$  (100) surface.

The electron density and differential charge density of the topmost surface layer atoms are shown in Fig. 7. The covalent interaction between  $\text{Li}_s$  and  $\text{O}_s$  atoms is weaker than that in bulk, which can be seen from the charge population. While the covalent interaction between  $\text{Ca}_s$  and  $\text{O}_s$  atoms is stronger than that in bulk.



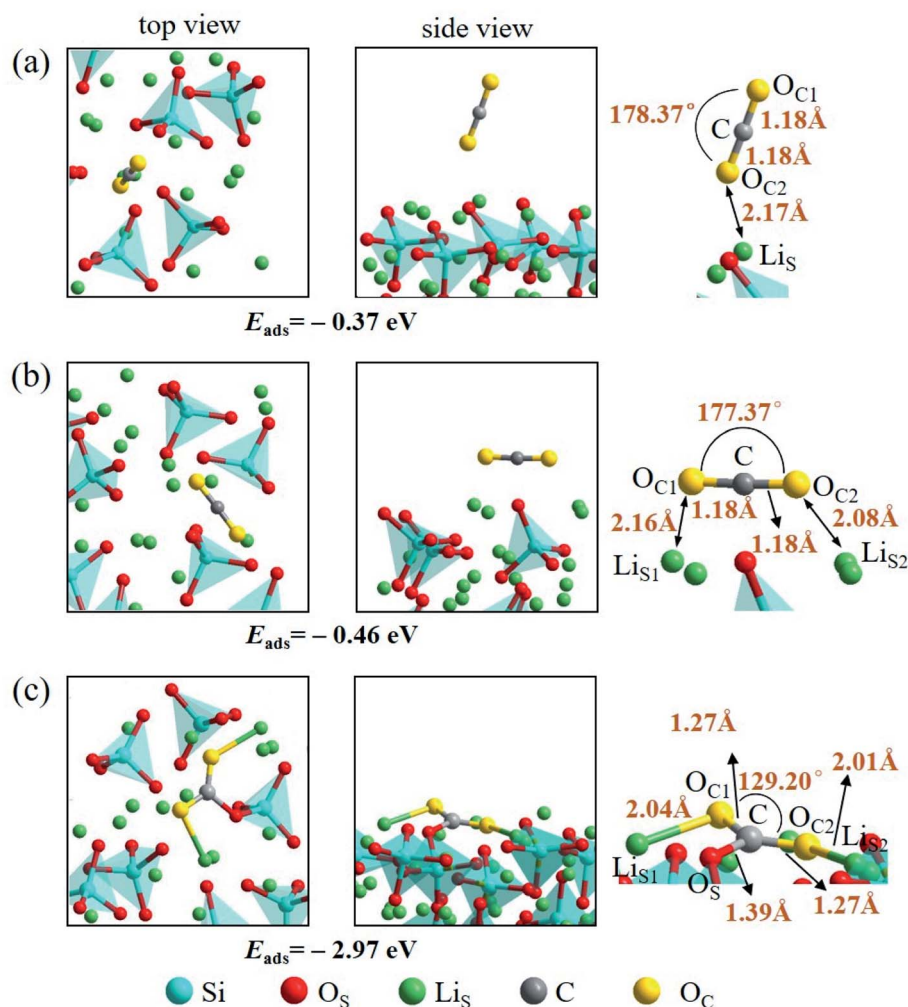


Fig. 9 Three configurations of an adsorbed CO<sub>2</sub> molecule on the Li<sub>4</sub>SiO<sub>4</sub> (010) surface: (a) along the normal to the surface, (b) parallel to the surface, (c) bent configuration.

Fig. 8 shows the Mulliken charge of atoms on the topmost surface layer. There is a considerable difference of the charge between bulk atoms (listed in ESI<sup>†</sup>) and atoms on the topmost surface layer. The positive charge of surface Li<sub>s</sub> and Ca<sub>s</sub> atoms increases, and the negative charge of the O<sub>s</sub> atoms increases compared with bulk atoms. And the deviation of Mulliken charge of surface Li<sub>s</sub> atoms from the bulk atoms is relatively large, whereas the Mulliken charge of surface Ca<sub>s</sub> and O<sub>s</sub> atoms differ from their bulk atoms slightly. Furthermore, the O<sub>s</sub> of Li<sub>4</sub>SiO<sub>4</sub> (010) surface carry more negative charge than Ca<sub>2</sub>SiO<sub>4</sub> (100) surface. According Lewis acid/base theory, O<sub>s</sub> atoms of Li<sub>4</sub>SiO<sub>4</sub> (010) surface are more basic and easier to lose electrons.

### 3.3. CO<sub>2</sub> adsorption on the surfaces

The adsorption energy ( $E_{\text{ads}}$ ) of a CO<sub>2</sub> molecule on Li<sub>4</sub>SiO<sub>4</sub> (010) surface and Ca<sub>2</sub>SiO<sub>4</sub> (100) surface is calculated according to the eqn (2):

$$E_{\text{ads}} = E_{\text{slab+CO}_2} - (E_{\text{slab}} + E_{\text{CO}_2}) \quad (2)$$

where  $E_{\text{slab+CO}_2}$  is the total energy of the surface with CO<sub>2</sub> adsorption,  $E_{\text{CO}_2}$  is the total energy of an isolated CO<sub>2</sub> molecule. The lower adsorption energy describes the stronger binding between the adsorbed CO<sub>2</sub> molecule and the surface, which reflects the stability of adsorption.

An isolated CO<sub>2</sub> molecule has linear configuration with the length of C–O bond of 1.18 Å. Three adsorption configurations are presented in this study when a CO<sub>2</sub> molecule is adsorbed on the Li<sub>4</sub>SiO<sub>4</sub> (010) surface as shown in Fig. 9. In the first configuration, the adsorbed CO<sub>2</sub> molecule almost remains linear configuration along the normal to the Li<sub>4</sub>SiO<sub>4</sub> (010) surface. The distance between O atom in CO<sub>2</sub> and the nearest Li<sub>s</sub> atom is 2.17 Å, and adsorption energy is –0.37 eV. In the second configuration shown in Fig. 9b, the adsorbed CO<sub>2</sub> molecule has a linear configuration parallel to the Li<sub>4</sub>SiO<sub>4</sub> (010) surface, and the adsorption energy is –0.46 eV. In the third configuration shown in Fig. 9c, the adsorbed CO<sub>2</sub> molecule is lying flat on the surface with the bent configuration. The C atom in CO<sub>2</sub> forms a bond with a surface O<sub>s</sub> atom with the O<sub>s</sub>–C distance of 1.39 Å, and its two oxygen atoms (O<sub>c</sub>) are



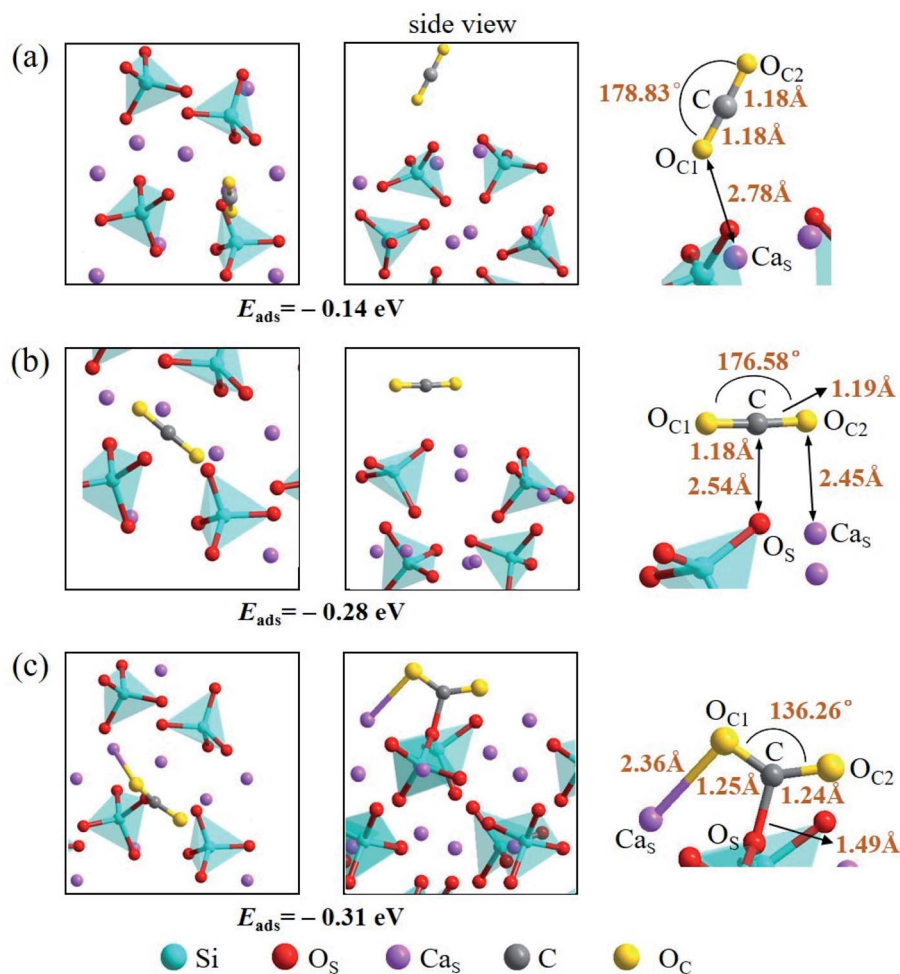


Fig. 10 Three configurations of an adsorbed CO<sub>2</sub> molecule on the Ca<sub>2</sub>SiO<sub>4</sub> (100) surface: (a) along the normal to the surface, (b) parallel to the surface, (c) bent configuration.

coordinated to the two surface Li<sub>s</sub> atoms, with the O<sub>C1</sub>-Li<sub>s</sub> and O<sub>C2</sub>-Li<sub>s</sub> distances are 2.04 and 2.01 Å, respectively. The adsorbed CO<sub>2</sub> molecule is bent with an O<sub>C1</sub>-C-O<sub>C2</sub> angle of 129.20° and the C-O<sub>C</sub> length of 1.27 Å. The adsorption energy is -2.97 eV. The third bent configuration of the adsorbed CO<sub>2</sub> on the Li<sub>4</sub>SiO<sub>4</sub> (010) surface is energetically favorable over the other two configurations.

There are also three adsorption configurations considered for an adsorbed CO<sub>2</sub> molecule on the Ca<sub>2</sub>SiO<sub>4</sub> (100) surface, as shown in Fig. 10. The first configuration, where an almost linearly CO<sub>2</sub> is adsorbed, is in vertical orientation and tilted slightly to the Ca<sub>2</sub>SiO<sub>4</sub> (100) surface, and the adsorption energy is -0.14 eV. The adsorbed CO<sub>2</sub> molecule is bent a little bit in the second configuration, which is in parallel orientation, and the adsorption energy is -0.28 eV. When the adsorbed CO<sub>2</sub> molecule lying on the Ca<sub>2</sub>SiO<sub>4</sub> (100) surface in a bent configuration shown in Fig. 10c, the distance of C-O<sub>s</sub> is 1.49 Å, and O<sub>C1</sub>-C-O<sub>C2</sub> angle is 136.26°. The bent configuration has the lowest value of adsorption energy, -0.31 eV in the third configurations.

It is found that the bent configuration consisting of a CO<sub>2</sub> molecule absorbed parallel along to the surface is the most thermodynamically stable among the three configurations considered here for both Li<sub>4</sub>SiO<sub>4</sub> and Ca<sub>2</sub>SiO<sub>4</sub> surfaces. Furthermore, the Li<sub>4</sub>SiO<sub>4</sub> (010) surface has greater adsorption to CO<sub>2</sub> than the Ca<sub>2</sub>SiO<sub>4</sub> (100) surface due to the stronger bond between C atom in CO<sub>2</sub> and the surface O<sub>s</sub> atom for Li<sub>4</sub>SiO<sub>4</sub>.

### 3.4. Partial density of state analysis

Considering that the adsorption energy of adsorbed CO<sub>2</sub> in bent configuration is the lowest, the PDOS calculations were only performed for this configuration, as shown in Fig. 11 and 12. It can be seen that the s and p orbitals of C and O<sub>C</sub> of adsorbed CO<sub>2</sub> molecule both move towards lower energy level and broaden compared with the isolated CO<sub>2</sub> molecule, indicating that CO<sub>2</sub> molecule becomes more stable after adsorption. C s and p orbitals of adsorbed CO<sub>2</sub> are hybridized with O<sub>s</sub> p orbitals, having bonding character between C and O<sub>s</sub> atoms. The states in the region between -3 and 0 eV are about 72% for O<sub>s</sub> p orbital for Li<sub>4</sub>SiO<sub>4</sub> (010) surface after adsorption, which is





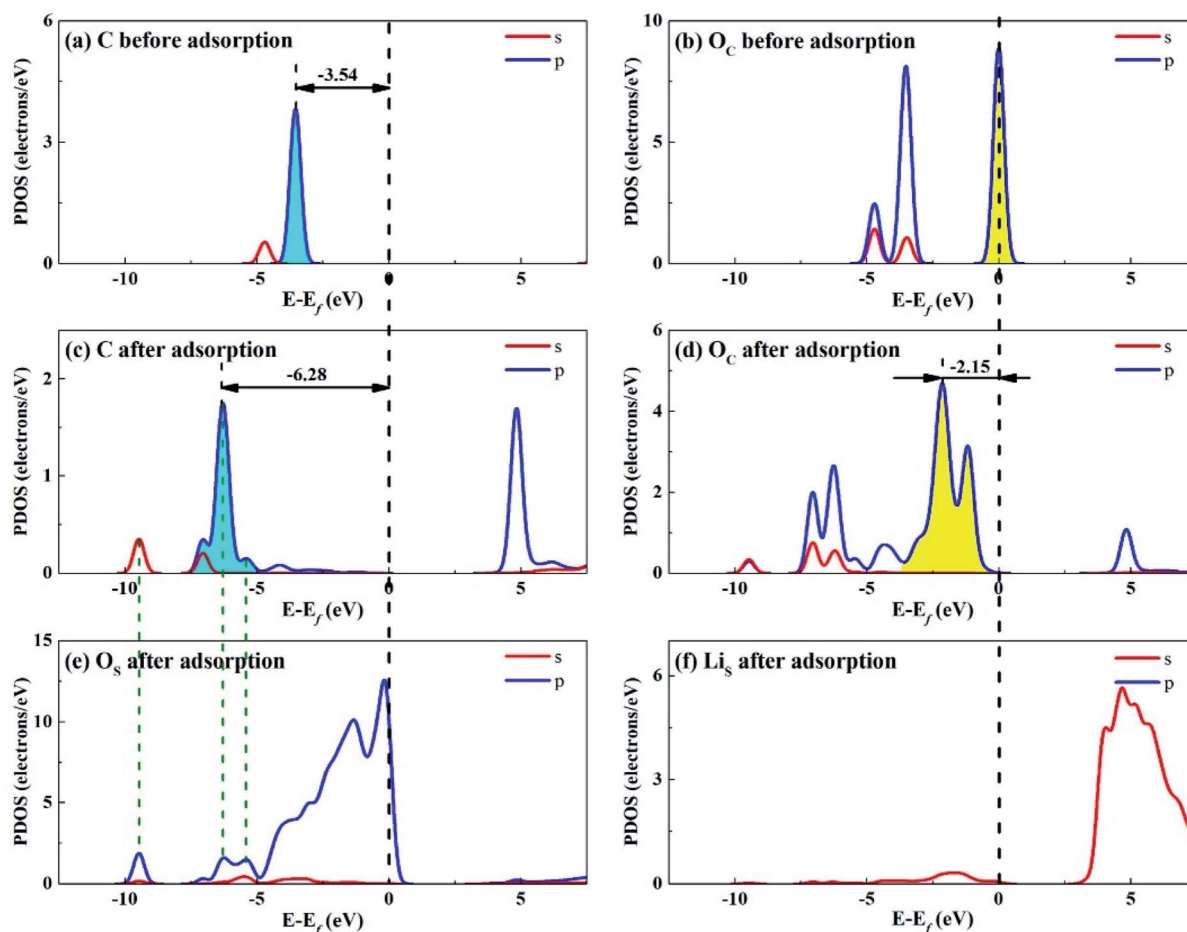


Fig. 11 PDOS analysis of (a) C and (b)  $O_C$  atoms of  $CO_2$  before adsorption, (c) C and (d)  $O_C$  atoms of  $CO_2$  and (e)  $O_S$  and (f)  $Li_S$  atoms of  $Li_4SiO_4$  (010) surface after adsorption.

decreased from 79% before adsorption, demonstrating that PDOS of  $O_S$  p orbitals is moved to lower energy level after  $CO_2$  adsorption. Furthermore, the PDOS peak of  $Li_S$  s orbital become weaker and broader after adsorption.

Fig. 12 shows the PDOS for  $CO_2$  and  $Ca_2SiO_4$  (100) surface after adsorption. Similarly, the s and p orbitals of C and  $O_C$  of adsorbed  $CO_2$  move towards lower energy and broaden, but not as far as  $Li_4SiO_4$  (010) surface. It can be deduced that  $CO_2$  adsorption on  $Li_4SiO_4$  (010) surface is more stable. The states in the region between  $-3$  and  $0$  eV are about 73% for  $O_S$  p orbitals for  $Ca_2SiO_4$  (100) surface. The PDOS peaks for  $Ca_S$  s orbital become weaker and broader after adsorption, similar to  $Li_S$  s orbital.

To better elucidate the different  $CO_2$  absorption behaviors of  $Li_4SiO_4$  (010) and  $Ca_2SiO_4$  (100) surfaces, the p-band centers of C and  $O_C$  in  $CO_2$  and  $O_S$  on the surfaces with and without  $CO_2$  adsorption were calculated, and the results were shown in Fig. 13. Comparing the p-band centers of  $O_S$  atoms on two clean surfaces, it can be found that the p-band center of  $O_S$  atoms on the  $Li_4SiO_4$  (010) surface is closer to the  $E_f$  than that of  $Ca_2SiO_4$  (100) surface, which means the  $O_S$  atoms of  $Li_4SiO_4$  (010) surface are more active and easier to transfer electrons to  $CO_2$

absorbed. When  $CO_2$  is adsorbed on the  $Li_4SiO_4$  (010) surface, it is obvious that p-band centers of C,  $O_C$  and  $O_S$  atoms are farther away from the  $E_f$ , indicating that  $CO_2$  adsorbed and  $O_S$  become stable. On the other hand, energy-down shift of the p-band centers of C,  $O_C$  and  $O_S$  atoms of  $Ca_2SiO_4$  (100) surface due to  $CO_2$  adsorption is much smaller compared with  $Li_4SiO_4$  (010) surface, probably leading to its higher absorption energy and less  $CO_2$  absorption.

### 3.5. Mulliken charge analysis

To understand the interactions and charge distributions associated with  $CO_2$  adsorbed with the most energetically favorable configurations on  $Li_4SiO_4$  (010) and  $Ca_2SiO_4$  (100) surfaces, a Mulliken charge analysis was performed. The detail date of Mulliken charges for  $CO_2$  and  $Li_4SiO_4$  (010) and  $Ca_2SiO_4$  (100) surfaces before and after adsorption were shown in Fig. 14. For  $CO_2$  adsorbed on  $Li_4SiO_4$  (010) surface, it is found that the Mulliken charge on a surface  $O_S$  atom changes from  $-1.33e$  to  $-0.86e$ , while the charges on the surface  $Li_{S_1}$  and  $Li_{S_2}$  atoms increase from  $0.93e$  to  $0.96e$ , and from  $0.93e$  to  $0.95e$ , respectively. It can be deduced that  $CO_2$  adsorption induces the net



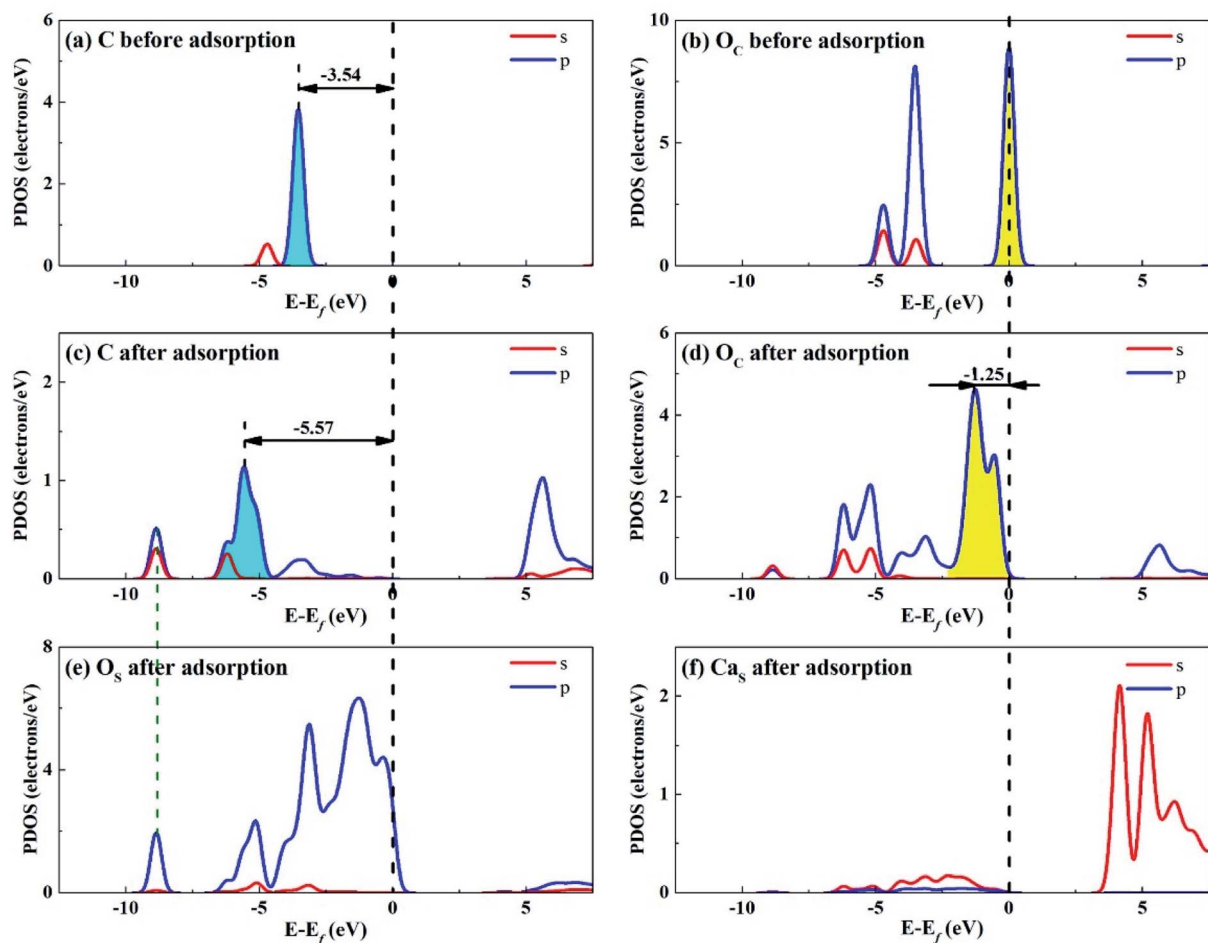


Fig. 12 PDOS analysis of (a) C and (b)  $O_C$  atoms of  $CO_2$  before adsorption, (c) C and (d)  $O_C$  atoms of  $CO_2$  and (e)  $O_S$  and (f)  $Ca_S$  atoms of  $Ca_2SiO_4$  (100) surface after adsorption.

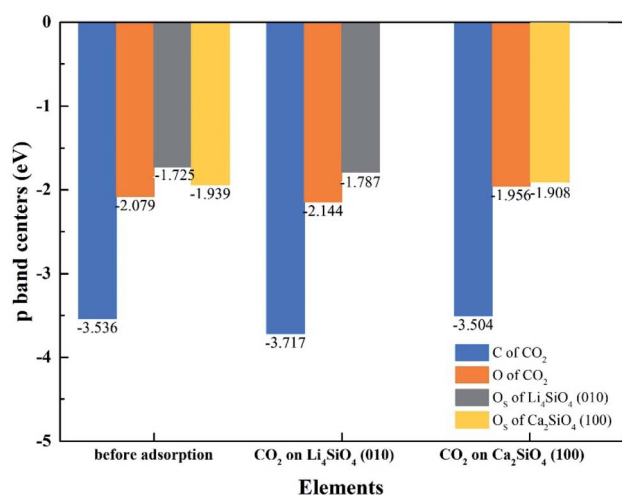


Fig. 13 The p-band centers of C 2p and O 2p orbitals of  $CO_2$ ,  $Li_4SiO_4$  (010) surface and  $Ca_2SiO_4$  (100) surface before and after adsorption.

electron loss of  $Li_4SiO_4$  (010) surface. On the other side, the Mulliken charge of C atom in  $CO_2$  adsorbed decreases from  $0.98e$  to  $0.76e$ , and the charges of  $O_{C1}$  and  $O_{C2}$  from  $-0.49e$  to  $-0.78e$  and  $-0.76e$ , respectively, which means that  $CO_2$  adsorbed gains the charges from  $Li_4SiO_4$  (010) surface.

In the case of  $CO_2$  adsorption on  $Ca_2SiO_4$  (100) surface, it is found that charge gain for C atom in  $CO_2$  adsorbed is similar to that on  $Li_4SiO_4$  (010) surface, but charges gained by  $O_{C1}$  and  $O_{C2}$  atoms are fewer. Furthermore, the Mulliken charge on an  $O_S$  atom on  $Ca_2SiO_4$  (100) surface changes from  $-1.12e$  to  $-0.88e$ , and the charge on the surface  $Ca_S$  from  $1.34e$  to  $1.40e$ . The net charge transfer from  $Ca_2SiO_4$  (100) surface to  $CO_2$  adsorbed is much less compared to that  $Li_4SiO_4$  (010) surface.

The charge population between C in  $CO_2$  adsorbed and a surface  $O_S$  atom was calculated to be 0.62 and 0.45 for  $Li_4SiO_4$  (010) and  $Ca_2SiO_4$  (100) surfaces, respectively. It can be deduced that the C- $O_S$  covalent interaction on  $Li_4SiO_4$  (010) surface is even stronger, which leads to the stronger adsorption of  $CO_2$ .



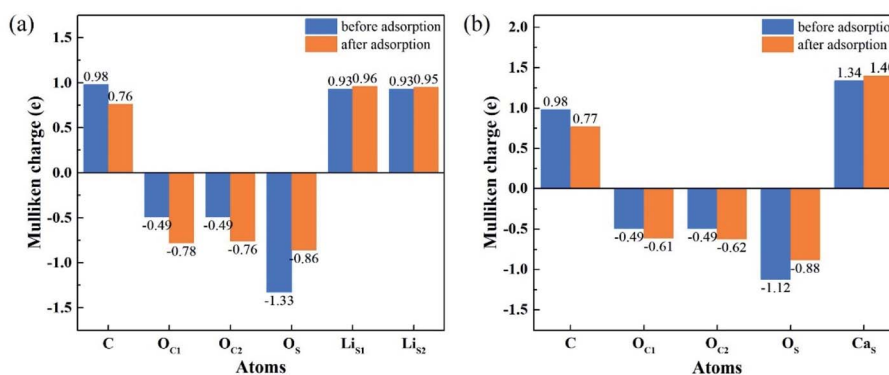


Fig. 14 Mulliken charge analysis of adsorbed CO<sub>2</sub> molecule and (a) Li<sub>4</sub>SiO<sub>4</sub> (010) surface, and (b) Ca<sub>2</sub>SiO<sub>4</sub> (100) surface before and after adsorption.

## 4. Conclusions

A density functional theory calculation was conducted to research the CO<sub>2</sub> adsorption on the Li<sub>4</sub>SiO<sub>4</sub> (010) and Ca<sub>2</sub>SiO<sub>4</sub> (100) surfaces. The bent configuration consisting of a CO<sub>2</sub> molecule adsorbed parallel along to the surface is the most thermodynamically favorable for Li<sub>4</sub>SiO<sub>4</sub> and Ca<sub>2</sub>SiO<sub>4</sub> surfaces. And the adsorption energy of Li<sub>4</sub>SiO<sub>4</sub> (010) surface is  $-2.97$  eV, more negative than Ca<sub>2</sub>SiO<sub>4</sub> (100) surface,  $-0.31$  eV. Li<sub>4</sub>SiO<sub>4</sub> (010) surface is more favorable for forming a stronger covalent bond between a surface O<sub>s</sub> atom to the C atom of CO<sub>2</sub> adsorbed and transferring more charges to adsorbed CO<sub>2</sub>. In addition, it was found that the Mulliken charge of O<sub>s</sub> atoms on the Li<sub>4</sub>SiO<sub>4</sub> (010) is more negative, and its p-band center is closer to the E<sub>f</sub>, which implies O<sub>s</sub> atoms of Li<sub>4</sub>SiO<sub>4</sub> (010) are more active and more likely serve as the electron donors with respect to Ca<sub>2</sub>SiO<sub>4</sub> (100) surface.

## Conflicts of interest

There are no conflicts to declare.

## Acknowledgements

This work was financially supported by the Natural Science Foundation of China (No. 51574163).

## References

- 1 R. Ben-Mansour, M. A. Habib, O. E. Bamidele, M. Basha, N. A. A. Qasem, A. Peedikakkal, T. Laoui and M. Ali, *Appl. Energy*, 2016, **161**, 225.
- 2 M. Seggiani, M. Puccini and S. Vitolo, *Int. J. Greenhouse Gas Control*, 2013, **17**, 25.
- 3 M. Kato, S. Yoshikawa and K. Nakagawa, *J. Mater. Sci. Lett.*, 2002, **21**, 485.
- 4 M. Kato, K. Nakagawa, K. Essaki, Y. Maezawa, S. Takeda, R. Kogo and Y. Hagiwara, *Int. J. Appl. Ceram. Technol.*, 2005, **2**, 467.
- 5 K. Wang, Z. Yin and P. Zhao, *Ceram. Int.*, 2016, **42**, 2990.

- 6 M. E. Bretado, V. G. Velderrain, D. L. Gutiérrez, V. Collins-Martínez and A. L. Ortiz, *Catal. Today*, 2005, **107–108**, 863.
- 7 K. Essaki and M. Kato, *J. Mater. Sci.*, 2005, **4**, 1.
- 8 R. Rodríguez-Mosqueda and H. Pfeiffer, *J. Phys. Chem.*, 2010, **114**, 4535.
- 9 M. J. Venegas, E. Fregoso-Israel, R. Escamilla and H. Pfeiffer, *Ind. Eng. Chem. Res.*, 2007, **46**, 2407.
- 10 S. Jeoung, J. H. Lee, H. Y. Kim and H. R. Moon, *Thermochim. Acta*, 2016, **637**, 31.
- 11 I. C. Romero-Ibarra, J. Ortiz-Landeros and H. Pfeiffer, *Thermochim. Acta*, 2013, **567**, 118.
- 12 V. L. Mejía-Trejo, E. Fregoso-Israel and H. Pfeiffer, *Chem. Mater.*, 2008, **20**, 7171.
- 13 G. V. Tomarov, Y. V. Petrov, A. A. Shipkov, O. A. Dovgii, V. N. Semenov and A. V. Mikhailov, *Therm. Eng.*, 2008, **55**, 154.
- 14 M. Zhao, J. Shi, X. Zhong, S. Tian, J. Blamey, J. Jiang and P. S. Fennell, *Energy Environ. Sci.*, 2014, **7**, 3291.
- 15 M. Zhao, Y. Song, G. Ji and X. Zhao, *Energy Fuels*, 2018, **32**, 5443.
- 16 Y. S. Kim and S. G. Kang, *Appl. Surf. Sci.*, 2019, **486**, 571.
- 17 A. Kumar, F. Ropital, T. de Bruin and B. Diawara, *Appl. Surf. Sci.*, 2020, **529**, 147127.
- 18 S. G. Kang, *J. CO<sub>2</sub> Util.*, 2020, **42**, 101293.
- 19 Y. Duan and K. Parlinski, *Phys. Rev. B: Condens. Matter Mater. Phys.*, 2011, **84**, 104113.
- 20 T. Tang, P. Chen, W. Luo, D. Luo and Y. Wang, *J. Nucl. Mater.*, 2012, **420**, 31.
- 21 X. Kong, Y. Yu, S. Ma, T. Gao, C. Xiao and X. Chen, *Chem. Phys. Lett.*, 2018, **691**, 1.
- 22 C. Qi, D. Spagnoli and A. Fourie, *Appl. Surf. Sci.*, 2020, **518**, 146255.
- 23 Q. Wang, H. Manzano, I. López-Arbeloa and X. Shen, *Minerals*, 2018, **8**, 1.
- 24 Q. Wang, F. Li, X. Shen, W. Shi, X. Li, Y. Guo, S. Xiong and Q. Zhu, *Cem. Concr. Res.*, 2014, **57**, 28.
- 25 M. C. Payne, M. P. Teter, D. C. Allan, T. A. Arias and J. D. Joannopoulos, *Rev. Mod. Phys.*, 1992, **64**, 1045.
- 26 J. P. Perdew, K. Burke and M. Ernzerhof, *Phys. Rev. Lett.*, 1996, **77**, 3865.



- 27 B. Hammer, *Phys. Rev. B: Condens. Matter Mater. Phys.*, 1999, **59**, 7413.
- 28 J. P. P. Ramalho, J. R. B. Gomes and F. Illas, *RSC Adv.*, 2013, **3**, 13085.
- 29 S. Grimme, J. Antony, S. Ehrlich and H. Krieg, *J. Chem. Phys.*, 2010, **132**, 154104.
- 30 D. J. Chadi, *Phys. Rev. B*, 1977, **16**, 1746.
- 31 B. G. Pfrommer, M. Côté, S. G. Louie and M. L. Cohen, *J. Comput. Phys.*, 1997, **131**, 233.
- 32 A. Belsky, M. Hellenbrandt, V. L. Karena and P. Lukschb, *Acta Crystallogr.*, 2002, **58**, 364.
- 33 R. Zhang, S. Ma, Q. Wang, C. Xiao, C. Zhang and T. Gao, *Ceram. Int.*, 2020, **46**, 8192.
- 34 Q. Guan, T. Gao, Y. Shen, S. Ma, T. Lu, X. Chen, C. Xiao and X. Long, *Int. J. Mod. Phys. B*, 2015, **29**, 1550128.
- 35 D. Tranqui, R. D. Shannont and H. Y. Chen, *Acta Crystallogr. B*, 1979, **35**, 2479.
- 36 C. Haitao, H. Xuefei and H. Weigang, *Rare Met. Mater. Eng.*, 2018, **47**, 729.
- 37 C.-J. Chan, W. M. Kriven and J. F. Young, *J. Am. Ceram. Soc.*, 1988, **71**, 713.
- 38 Y. J. Kim, I. Nettleship and W. M. Kriven, *J. Am. Ceram. Soc.*, 1992, **75**, 2407.
- 39 A. V. Marenich, S. V. Jerome, C. J. Cramer and D. G. Truhlar, *J. Chem. Theory Comput.*, 2012, **8**, 527.
- 40 K. H. Jost, B. Ziemer and R. Seydel, *Acta Crystallogr.*, 1977, **33**, 1696.
- 41 W. Tao, C. Zhu, Q. Xu, S. Li, X. Xiong, H. Cheng, X. Zou and X. Lu, *ACS Omega*, 2020, **5**, 20090.
- 42 E. Durgun, H. Manzano, P. V. Kumar and J. C. Grossman, *J. Phys. Chem. C*, 2014, **118**, 15214.
- 43 W.-B. Zhang, C. Chen and S.-Y. Zhang, *J. Phys. Chem. C*, 2013, **117**, 21274.

